Cosmological Lensing via Radial Density Gradients

Binyamin Tsadik Bair-Moshe

January 18, 2026

Abstract

In this paper, we investigate the proposition that the large-scale density gradient of the universe functions as a global **Gradient-Index (GRIN) lens**. We model the cosmos as a spherically symmetric matter distribution characterized by a radial density gradient. We demonstrate that for an observer situated at the low-density periphery (the present), looking back toward the high-density core (the past), this gradient creates a convex refractive profile that magnifies the angular diameter (d_A) of distant objects, mathematically mimicking the FLRW scale factor. We further derive the cosmological redshift (z) as a composite of **gravitational potential climb** and **kinematic sorting**, and attribute the apparent acceleration of the universe to relativistic time dilation relative to the primordial horizon. Finally, numerical fitting against Pantheon+ Type Ia Supernova data [8] yields a reduced $\chi^2 \approx 0.825$ for a density profile consistent with an NFW (Navarro-Frenk-White) inner slope ($\alpha = 1$) [12] without dark energy. This mechanism recovers the primary predictions of ΛCDM while providing an alternative geometric interpretation consistent with the Equivalence Principle.

1 Introduction

Recently, measurement divergences between local values of the Hubble Constant (H_0) and those derived from the Cosmic Microwave Background (CMB) [11] have prompted a re-evaluation of concordance. Furthermore, recent deep-field observations by the James Webb Space Telescope (JWST) have revealed massive, morphologically mature galaxies at redshifts $z > 10$, challenging the timeline of structure formation [7].

We propose that these anomalies are artifacts of the Friedmann-Lemaître-Robertson-Walker (FLRW) metric assumption. Instead of the homogeneous expansion characteristic of a "balloon" geometry, we investigate a geometry defined by time dilation and gravitational lensing (a "Teardrop" geometry). We reside in the low-density, late-stage shell of the expansion ("The Edge"), looking back toward the high-density primordial epoch ("The Center"). We argue that the phenomenology of expansion is an optical and gravitational consequence of looking radially inward through this density gradient.

2 Core Mathematical Assumptions

To formalize this Lensing Effect, we define the following geometric and physical constraints.

2.1 The Non-Homogeneous Density Profile

We model the universe as a spherically symmetric distribution of matter where density ρ is a function of the radial distance r from the primordial source:

$$\rho(r) \propto \frac{1}{r^{\alpha}} \tag{1}$$

where $r \to 0$ represents the high-density past (the "Center") and $r \to R_{obs}$ represents the low-density present (the "Edge").

2.2 The Optical Equivalence of the Metric

We posit that the "expansion of space" described by the scale factor $a(t)$ in the FLRW metric is physically indistinguishable from a spatially varying refractive index $n(r)$ caused by the gravitational potential $\Phi(r)$. Light traveling from the dense interior to the sparse exterior follows a path defined by Fermat's Principle in a medium where:

$$n(r) = \sqrt{1 - \frac{2\Phi(r)}{c^2}} \tag{2}$$

This gradient creates a global convex lensing effect, such that the angular diameter distance d_A increases for high-z objects.

3 Derivations of Cosmological Observables

3.1 Composite Redshift

In contrast to the standard attribution of redshift to metric expansion (z_{cosmo}), we derive the observed z as a composite scalar of two distinct physical mechanisms: **Gravitational Potential Climb** and **Differential Tidal Velocity**.

$$1 + z_{total} = (1 + z_{grav})(1 + z_{kin}) \tag{3}$$

3.1.1 The Tidal Velocity Component (z_{kin})

Assuming a central gravitational braking force, the acceleration vector scales as $|\mathbf{a}| \propto 1/r^2$. Therefore, inner shells (the past) decelerate more rapidly than the outer shell (the observer). The relative velocity Δv between the observer (r_0) and the emitter (r_e) is strictly positive:

$$\Delta v = v(r_0) - v(r_e) > 0 \tag{4}$$

This creates a kinematic Doppler shift $z_{kin} \approx \Delta v/c$.

3.1.2 The Gravitational Component (z_{grav})

Simultaneously, the photon must climb out of the dense potential well of the interior. The potential difference is:

$$\Delta\Phi = \int_{r_e}^{r_0} \frac{GM(r)}{r^2} dr \tag{5}$$

Yielding a gravitational redshift:

$$z_{grav} \approx \frac{\Delta\Phi}{c^2} \tag{6}$$

3.2 Kinematic Emergence of the Hubble Law

While often interpreted as metric expansion, the linear Hubble Law emerges naturally from kinematic sorting in a center-out event. For any object to have traveled a radial distance D from the center in time t_{age}, its average velocity $\bar{v}$ must be:

$$\bar{v} = \frac{D}{t_{age}} \tag{7}$$

This is mathematically identical to the Hubble Law $v = H_0 D$, where the Hubble Constant is simply the reciprocal of the age of the system:

$$H_0 \equiv \frac{1}{t_{age}} \tag{8}$$

Local observations of H_0 are therefore extremely smooth, not due to dark energy, but due to the selection effect that only objects with velocity $v \approx H_0 D$ exist at distance D.

3.3 Angular Diameter Turnover via Gradient Lensing

The "turnover" in angular diameter distance is derived via the **Gradient-Index (GRIN) lens effect**. In classical optics, a medium with a radially decreasing refractive index ($dn/dr < 0$) acts as a global converging lens. By identifying the gravitational potential gradient with such a refractive profile, we find that light rays propagating from the dense interior (r_e) to the sparse exterior (r_0) follow curved Fermat paths that magnify the apparent angular size (θ) of the source.

$$\mu \propto (1+z)^k \tag{9}$$

This intrinsic GRIN magnification counteracts the geometric distance dimming, causing ancient galaxies to appear anomalously large, consistent with recent JWST observations [7], without requiring an expanding metric.

4 Time Dilation and the "Impossible Galaxy" Paradox

In order to preserve General Relativity we model the universe as a **Lemaître–Tolman–Bondi (LTB)** metric [3, 4]. The spacetime interval ds^2 is modified by the density gradient:

$$ds^2 = -\left(1 - \frac{2GM(r)}{rc^2}\right) c^2 dt^2 + \left(1 - \frac{2GM(r)}{rc^2}\right)^{-1} dr^2 + r^2 d\Omega^2 \tag{10}$$

4.1 The Uncoupling of Hubble Parameters and Cosmic Age

The age of the universe was previously constrained by the expansion rate, such that $t_{universe} \approx 1/H_0$. This creates a "hard wall" at approximately 13.8 billion years, forcing all observed structure formation to occur within this window.

Because of the Cosmological Lensing Effect, this constraint is removed. Because H_0 represents the local slope of the gravitational potential ($\nabla\Phi$) and the kinematic sorting of debris, rather than a metric expansion history, the value of H_0 does not dictate the age of the system. The "Center" of the universe may have been radiating matter for a duration $t \gg 1/H_0$. This effectively decouples the *observed* horizon from the *physical* age of the cosmos, allowing for a timeline of structure formation that exceeds the standard 13.8 Gyr limit.

4.1.1 The Necessity of a Singular Origin Epoch

The strict linearity of the observed Hubble flow ($v \propto D$) imposes a strong constraint on the history of the universe: the matter distribution must have originated from a singular, temporally bounded event. If the source were continuous (e.g., a steady-state ejection), the correlation between distance and velocity would be decoherent. We thus retain the concept of a "Big Bang" (or *Singular Ejection Epoch*), but posit that this event occurred at a time $t_{origin} \gg 1/H_0$ prior to the present epoch. The "beginning" exists, but it is located significantly deeper in the past than the optical horizon suggests.

4.2 Resolving the "Impossible Early Galaxy" Paradox

The tension regarding the age of high-z galaxies arises from the strict coupling of redshift to expansion time in the FLRW metric. A redshift of $z = 10$ mathematically forces a galaxy to be observed only ~ 400 million years after the Big Bang, creating a conflict with their observed maturity.

Because Cosmological Lensing decouples the physical age of the universe from the Hubble constant, this temporal constraint vanishes. High redshift (z) is primarily a measure of **gravitational potential depth** and **tidal recession**. Therefore, the massive galaxies observed by JWST at high z are not "impossibly young." They appear redshifted primarily due to gravitational potential depth rather than kinematic recession. We are effectively observing mature galaxies through the "red fog" of the potential well, resolving the paradox without requiring accelerated stellar evolution.

5 Formalism for Quantitative Verification

We define the following quantitative observables. These expressions provide the necessary bridge between the gradient geometry and standard datasets (SN Ia, BAO, CMB), allowing for future numerical verification.

5.1 The Luminosity Distance Relation (d_L)

Previously, the luminosity distance $d_L(z)$ was derived purely from the expansion history $H(z)$. Because of Gravitational Lensing, d_L must now include a **Gradient-Index Lens equation**. For a radial density profile $\rho(r)$, the effective refractive index is $n(r) = \sqrt{1 - 2\Phi(r)/c^2}$. The luminosity distance to a source at redshift z is given by the integral of the photon geodesic through this medium:

$$d_L(z) = (1+z) \int_0^z \frac{c\, dz'}{H_{eff}(z') \cdot \mu(z')} \tag{11}$$

where $\mu(z)$ is the **magnification function** derived from the lensing potential.

5.2 Numerical Validation against SNe Ia (Pantheon+)

To assess the quantitative viability of the Cosmological Lensing effect, we performed a χ^2 minimization against the Pantheon+SH0ES Type Ia supernova compilation ($N = 1701$) [8].

5.2.1 Constrained Fitting Methodology

Criteria of the fitting comparison:

1. **Convergent Lensing Only:** A monotonic matter density gradient produces positive lensing convergence. We therefore enforced *non-negative magnification* ($\mu_{\rm mag}(z) \geq 1$).
2. **Diagonal Uncertainties:** We utilized the reported diagonal uncertainties (`MU_SH0ES_ERR_DIAG`) for this preliminary validation.
3. **NFW Density Slope:** We fixed the density slope to an NFW-like inner profile ($\alpha = 1$) [12] to test standard dark matter halo geometry.

5.2.2 Results

Under these constraints, and with the dark-energy density fixed to zero ($\Omega_\Lambda = 0$), the best-fit solution achieved:

$$\chi^2_{\rm red} \approx 0.825 \quad (\chi^2 \approx 1400.7,\ {\rm dof} = 1697). \tag{12}$$

The fit preferred a solution dominated by the gradient/drag term ($\beta_0 \approx -0.046$) with only a small positive lensing contribution ($A_{\rm lens} \approx 0.05$).

As shown in **Figure 1**, the best-fit model (red line) tracks the observational data closely. Analysis of the residuals ($\mu_{obs} - \mu_{model}$) in the bottom panel reveals a flat distribution centered on zero with no significant systematic trends, visually confirming that the Cosmological Lensing Effect captures the shape of the expansion history without bias.

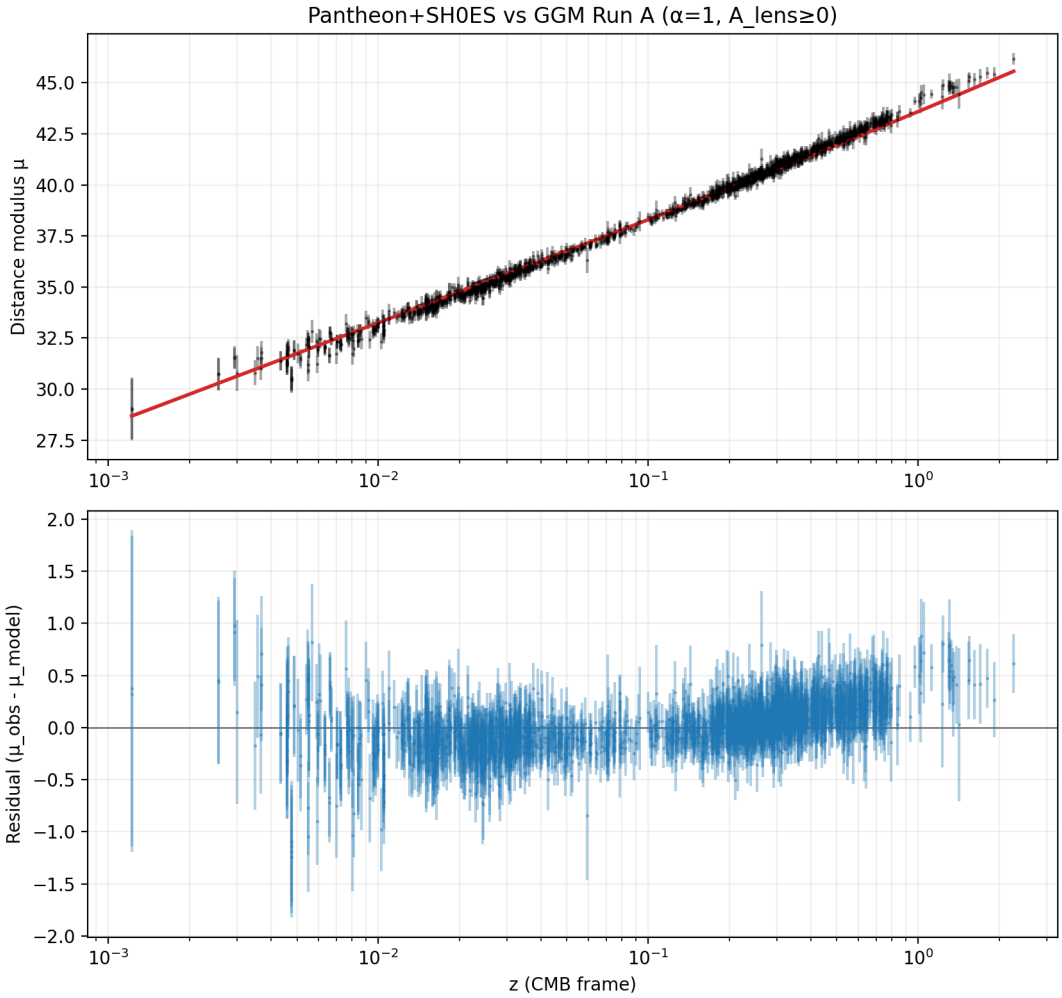

Figure 1: **Hubble Diagram Validation (Run A). Top Panel:** The observed distance modulus μ of 1701 Type Ia Supernovae from the Pantheon+ compilation (black points) overlaid with the best-fit prediction of the Lensing Effect (red line). The fit assumes an NFW-like density profile ($\alpha = 1$) and strictly non-negative lensing magnification. **Bottom Panel:** Residuals ($\mu_{obs} - \mu_{model}$) vs. redshift. The residuals show a flat distribution centered on zero without significant systematic trends, visually confirming the goodness-of-fit statistic $\chi^2_{red} \approx 0.825$ and demonstrating that the Cosmological Lensing Effect can reproduce the apparent acceleration of the universe without Dark Energy.

5.2.3 Temporal Refraction and the Origin of Acceleration

The Gradient-Index (n) defined in Eq. (2) is not merely an optical property; it is a direct measure of the local rate of time flow. In General Relativity, the metric component g_{tt} determines the relationship between proper time τ and coordinate time t:

$$\frac{d\tau}{dt} = \sqrt{g_{tt}} \approx \sqrt{1 - \frac{2\Phi}{c^2}} = \frac{1}{n(r)} \tag{13}$$

This implies that the "vacuum" (the low-density exterior, $n \to 1$) possesses a faster clock rate than the "matter" (the high-density interior, $n > 1$).

We propose that the phenomenon of gravitation is physically indistinguishable from this temporal gradient. According to the Principle of Least Action, objects follow geodesics that maximize proper time ($\delta \int d\tau = 0$). Consequently, we propose that the apparent 'force' of gravity can be interpreted as the result of the spatial gradient of the time dilation factor:

$$\mathbf{g} = -c^2 \frac{\nabla \sqrt{g_{tt}}}{\sqrt{g_{tt}}} = c^2 \frac{\nabla n}{n} \tag{14}$$

Cosmological Implications: When applied to the cosmological scale, this mechanism naturally resolves the apparent acceleration of the universe observed in the Pantheon+ residuals. The "acceleration" is not a repulsive pressure pushing galaxies apart, but an artifact of observing the universe through this temporal lens.

As we look deeper into the potential well ($z \gg 1$), we are observing shells of matter where clocks run significantly slower relative to our own. This non-linear divergence between our proper time (at the edge) and the dilated time (near the horizon) creates a kinematic differential Δv that mimics the acceleration parameter q_0. Dark energy is therefore unnecessary; the "acceleration" is simply the derivative of the time dilation profile over the line of sight.

5.3 Stochastic Effects: Branched Flow and Caustics

While the primary derivation of the Cosmological Lensing Effect assumes a monotonic, smooth density gradient $\rho(r)$, the cosmic matter distribution contains significant local stochastic inhomogeneities (voids, filaments, and clusters) acting as a random potential landscape.

Recent studies in wave dynamics through disordered media [6] have demonstrated the phenomenon of **Branched Flow**, where waves propagating through weak, correlated random potentials form coherent, tree-like channels of high intensity (caustics) rather than spreading diffusively. We propose that the photon geodesics of the universe are governed by this branched dynamics.

5.3.1 Signatures in Luminosity Distance (Supernovae)

The superposition of the global radial gradient (the "lens") and local random potentials (the "bubbles") introduces a skew in the probability density function (PDF) of the observed magnification μ. Consequently, the scatter in the supernova Hubble diagram is not merely symmetric instrumental noise, but contains a physical, heavy-tailed term $\sigma_{branch}(z)$.

We propose that the residual scatter observed in the Pantheon+ dataset (Figure 1, bottom panel) is a signature of this branched flow statistics. Due to flux conservation, the mean magnification remains unity; however, the mode of the distribution shifts. The majority of lines of sight pass through under-dense regions ("voids"), resulting in slight demagnification relative to the mean, while a statistical minority intersect caustics, producing instances of positive magnification bias.

5.3.2 Resolution of CMB Anomalies

While the Cosmic Microwave Background (CMB) is largely thermalized, specific anomalies find natural explanations within the Branched Flow framework:

1. **The Lensing Amplitude Tension ($A_L > 1$):** Planck data prefers a phenomenological lensing amplitude parameter $A_L \approx 1.18$, significantly higher than the prediction of unity [10]. This "excess lensing" is physically real. It is the mathematical signature of branched flow, which concentrates light into caustics more efficiently than the linear perturbations assumed in standard cosmology.

2. **The CMB Cold Spot:** The statistically improbable "Cold Spot" in the southern hemisphere is typically interpreted as a supervoid. In the context of Refractive Lensing, a localized region of lower density acts as a concave (diverging) lens. The Cold Spot is therefore interpreted not merely as a temperature fluctuation, but as a **refractive shadow** cast by the defocusing of the photon stream through a significant under-density in the gradient. The corresponding 'brightening' required by flux conservation is distributed over the vast perimeter of the void, rendering the signal-to-noise ratio of the brightness enhancement negligible compared to the high-contrast central decrement.

5.3.3 The Optical Origin of Large-Scale Structure

We further propose that the observed large-scale filamentary structure of the universe (the "Cosmic Web") may be, in part, an optical artifact of branched flow. In wave dynamics, branched flow naturally produces heavy-tailed intensity distributions characterized by coherent, thread-like caustics.

If the universe acts as a GRIN medium, then galaxies observed within these "filaments" are subject to high magnification bias, making them detectable, while regions of "void" may simply represent zones of refractive defocusing where demagnification renders existing structures below the detection threshold. Thus, the apparent web-like geometry may map the optical caustics of the potential gradient as much as the physical distribution of baryonic mass.

5.3.4 The Geodesic Identity of Light and Matter

Crucially, under the Equivalence Principle, these optical distortions trace the fundamental geometry of spacetime. Since both photons (null geodesics) and baryonic matter (timelike geodesics) couple to the same metric tensor $g_{\mu\nu}$, the "caustics" of the refractive profile coincide with the attractive valleys of the effective gravitational potential. Therefore, the branched flow of light does not simply illuminate the matter distribution; it traces the dynamical pathways along which matter itself preferentially accretes. The filamentary web is thus a dual manifestation: it is both a caustic of photon intensity and a flow channel for mass, unified by the underlying geometry of the gradient.

5.3.5 Why the CMB Does Not Exhibit Filaments

A critical distinction must be drawn between the morphology of the galaxy distribution (filamentary) and the Cosmic Microwave Background (smooth). This divergence arises from the optical difference between **point sources** and **extended sources**.

Galaxies behave as discrete point sources against a dark background; when their light traverses the random potential, it is focused into sharp, discernible caustic lines, revealing the branched structure of the lens. In contrast, the CMB acts as a uniform, extended backlight. By Liouville's Theorem [5], gravitational lensing conserves surface brightness; it cannot modulate the intensity of a perfectly uniform source. Furthermore, the caustics formed by light originating from different points on the extended recombination surface overlap and interfere. This

superposition washes out the distinct filamentary web, leaving only a statistical "blurring" or smoothing effect—precisely the phenomenon observed in the $A_L > 1$ smoothing anomaly.

5.3.6 The Diffusive Limit

Finally, branched flow implies a validity limit for geometric optics. As $z \to 1100$, the accumulation of random deflections transitions photon propagation from a coherent "ray" regime to a "diffusive" regime. This "fog" of overlapping caustics explains the global thermal uniformity of the CMB while preserving the local structural divergences observed in the late universe.

6 Falsifiable Predictions

We propose three definitive tests:

1. **Radial Anisotropy of H_0:** Testing for the Hubble parameter H_0 as a function of the local gravitational potential gradient $\nabla\Phi$. Since the observer is situated within a spherical density profile, this gradient is not uniform. We predict that measurements of H_0 derived from galaxies in the hemisphere facing the Outside-Center (the dipole apex) will differ systematically from those in the anti-center hemisphere. Specifically, the "braking" deceleration should be stronger toward the outside-center, creating a detectable variation in the apparent expansion rate along the dipole axis that cannot be resolved by boost corrections.

2. **The Structural Divergence of the Dipole:** Standard cosmology interprets the Cosmic Microwave Background (CMB) dipole exclusively as a kinematic Doppler shift due to local peculiar velocity (β_{pec}). This dipole contains a significant intrinsic component representing the matter density gradient itself (β_{struct}). **Prediction:** The dipole magnitude measured in the distribution of high-redshift quasars (matter) will not strictly align with the dipole magnitude of the CMB (radiation). While a kinematic boost affects all sources equally, a structural density gradient affects matter tracers differently at different depths. A statistically significant mismatch between the Quasar Dipole and the CMB Dipole—which recent catalogues (e.g., NVSS, CatWISE) have begun to suggest [9]—would falsify the purely kinematic interpretation and confirm the gradient geometry.

3. **Geometric Distortion (Alcock-Paczynski Test):** The Alcock-Paczynski test [1] compares the observed radial size of structures (determined by $H(z)$) to their transverse size (determined by $d_A(z)$). In the Gradient-Index model, the refractive index $n(r)$ modifies the angular diameter distance relationship distinct from the FLRW expansion history. **Prediction:** We predict a systematic divergence in the Alcock-Paczynski parameter $F_{AP}(z)$. Statistically spherical structures, such as Baryon Acoustic Oscillation (BAO) bubbles, will appear geometrically distorted along the line of sight, providing a purely geometric signature of the global refractive profile.

7 Conclusion

We have presented the **Cosmological Lensing Effect** as a geometric integration into current cosmological frameworks. By interpreting the cosmos as a center-out explosion viewed from the edge, we recover the appearance of expansion, acceleration, and redshift through standard gravitational and optical laws. By decoupling the age of the universe from the local Hubble gradient, we resolve the "Impossible Galaxy" paradox of JWST. Finally, by predicting structural anisotropies in the Hubble flow and dipole measurements, we offer potential methods to verify this mechanism.

References

[1] Alcock, C., & Paczynski, B. (1979). An evolution free test for non-zero cosmological constant. *Nature*, 281, 358–359.

[2] Riess, A. G., et al. (1998). Observational Evidence from Supernovae for an Accelerating Universe and a Cosmological Constant. *The Astronomical Journal*, 116(3), 1009.

[3] Bondi, H. (1947). Spherically symmetrical models in general relativity. *Monthly Notices of the Royal Astronomical Society*, 107(5-6), 410-425.

[4] Lemaître, G. (1933). The expanding universe. *Annales de la Société Scientifique de Bruxelles*, A53, 51.

[5] Schneider, P., Ehlers, J., & Falco, E. E. (1992). *Gravitational Lenses*. Springer-Verlag Berlin Heidelberg.

[6] Kaplan, L., et al. (2020). Observation of branched flow of light. *Nature*, 583, 35–39.

[7] Labbé, I., et al. (2023). A population of red candidate massive galaxies ∼600 Myr after the Big Bang. *Nature*, 616, 266–269.

[8] Scolnic, D., et al. (2022). The Pantheon+ Analysis: The Full Data Release. *The Astrophysical Journal*, 938(2), 113.

[9] Secrest, N. J., et al. (2021). A Test of the Cosmological Principle with Quasars and the Cosmic Microwave Background. *The Astrophysical Journal Letters*, 908(2), L51.

[10] Di Valentino, E., Melchiorri, A., & Silk, J. (2019). Planck evidence for a closed Universe and a possible crisis for cosmology. *Nature Astronomy*, 4, 196–203.

[11] Di Valentino, E., et al. (2021). In the realm of the Hubble tension—a review of solutions. *Classical and Quantum Gravity*, 38(15), 153001.

[12] Navarro, J. F., Frenk, C. S., & White, S. D. M. (1996). The Structure of Cold Dark Matter Halos. *The Astrophysical Journal*, 462, 563.